Molecular Crystals and Liquid Crystals
Publication details, including instructions for authors and subscription information:
http://www.tandfonline.com/loi/gmcl20

Investigations of Electrical and Electro-Optical Properties of Liquid Crystal/Copolymer-Clay Nanostructured Systems

Doina Manaila Maximean [a], Constantin Rosu [a], Ligia Frunza [b], Paul Ganea [b], Dan Donescu [c] & Marius Ghiurea [c]

[a] Physics Department II, University "Politehnica Bucuresti", Bucharest, Romania

[b] National Institute of Materials Physics, Magurele, Romania

[c] ICECHIM, Bucharest, Romania

Version of record first published: 16 Jun 2011

To cite this article: Doina Manaila Maximean, Constantin Rosu, Ligia Frunza, Paul Ganea, Dan Donescu & Marius Ghiurea (2011): Investigations of Electrical and Electro-Optical Properties of Liquid Crystal/Copolymer-Clay Nanostructured Systems, Molecular Crystals and Liquid Crystals, 546:1, 143/[1613]-155/[1625]

To link to this article: http://dx.doi.org/10.1080/15421406.2011.571946

Mol. Cryst. Liq. Cryst., Vol. 546: pp. 143/[1613]–155/[1625], 2011

ISSN: 1542-1406 print/1563-5287 online
DOI: 10.1080/15421406.2011.571946

Investigations of Electrical and Electro-Optical Properties of Liquid Crystal/Copolymer-Clay Nanostructured Systems

DOINA MANAILA MAXIMEAN,[1] CONSTANTIN ROSU,[1] LIGIA FRUNZA,[2] PAUL GANEA,[2] DAN DONESCU,[3] AND MARIUS GHIUREA[3]

[1]Physics Department II, University "Politehnica Bucuresti", Bucharest, Romania
[2]National Institute of Materials Physics, Magurele, Romania
[3]ICECHIM, Bucharest, Romania

We obtained a new system containing nematic liquid crystal doped with nanostructured copolymer-clay particles. The clay (Cloisite-type) was modified by copolymerization of maleic anhydride and divinyl benzene and the nanocomposite has intercalated structure. Current-voltage characteristics of the liquid crystal/copolymer-clay systems were analyzed and the electro-optical response at heating –cooling cycles for different applied electric fields is discussed. Dielectric spectroscopy measurements in the low frequency domain have shown different regimes of its temperature dependence as function of the sample nature and the applied voltage. Comparison is made with the bulk liquid crystal. Changes of the phase transition temperature are thus revealed.

Keywords Copolymer-clay nanosystem; current-voltage curve; impedance spectroscopy; liquid crystal; optical transmission

1. Introduction

In the last decade liquid crystal/montmorillonite clay nanocomposites have been studied in search of new materials with improved electro-optical properties. Clays have been increasingly selected as fillers in polymer composite research and industrial applications [1–4]. In dispersions, the particles form internal interfaces with large specific surface, making possible to stabilize different director configurations. Properties of heterogeneous liquid crystal-clay nanocomposites are of great interest [5] and complex system such as Polymer Dispersed Liquid Crystals Hybridized with nanoclays have also been studied [6,7].

Address correspondence to Doina Manaila Maximean, Physics Department II, University "Politehnica Bucuresti", Spl. Independentei 313, R-060042, Bucharest, Romania. Tel.: +40722215089; Fax: +40214029120; E-mail: educmat2na@yahoo.com

For a good interaction with the liquid crystals, particles should present on their surface compatible functional groups or groups capable of strong physico-chemical interactions. Thus, surfactants [8,9] or modifications of the montmorillonite by hydrophobic organic substances [5] have been intensely used.

Polymer–clay nanocomposites are formed by dispersion of the clay nanometer silicate layers into polymers. The key to formation of nanocomposites with property improvements is to facilitate the dispersion of single silicate layer into the polymer matrix.

In this paper are presented new nanostructured systems containing a known nematic liquid crystal and newly synthesized copolymer-clay particles [10]. The doping particles are surface surfactant free and the good compatibility with the LC is ensured by chemical groups integrated in their structure, during the polymerization. The systems to be investigated were obtained by dispersing the polymer-clay nanocomposite in the nematic liquid crystal K15 (Merck) [11]. The electrical and electro-optical properties of nanocomposites have been explored and compared with the behavior of the pure liquid crystal and related systems based on a mixture of nematic liquid crystals [12].

2. Experimental

2.1. *Synthesis of Copolymer-Clay Nanocomposite Particles*

Cloisite layered silicates are structured in tactoids (parallel orientated layers), which are regularly stacked along the [001] or out-of-plane direction. Cloisite was used as nanofiller for the further generated polymer matrix. Na cloisite (as supplied by SothernClay Product Inc.) has Na^+ interstitial cations, and the interlayer distance is 1.17 nm. The synthesis conditions of the nanostructured composites have been described previously in detail [11]; in principal, these are as follows: first 1 g Na Cloisite was dispersed in a mixture (40/60 v/v) of methyl ethyl cetone and heptane, then 4 g maleic anhydride (MA), 4 g divinyl benzene (DVB) were added [10]. The polymerization reaction was performed at 70°C for 4 hours, adding 0.2 g azoisobutytironitrile (AIBN) as initiator, twice, every 2 hours. Finally the solvent system was removed through evaporation. The final functionalized copolymer-clay nanocomposite (DVB-MA/clay) has intercalated structure according to X Ray Diffraction (XRD) pattern [10]. To ensure a better interaction of the nanostructured organic-inorganic particles with liquid crystal molecules, a reactive surfactant, namely the maleic monoester of $MEMNPO_4$ [10] was included in the synthesized particles. The nonylphenol group of $MEMNPO_4$ is compatible with the phenyl groups existing in the liquid crystal K15. A so called "hairy" particle [4], has thus been obtained (see Table 1 for the particle dimensions).

The copolymer-clay nanocomposite was dispersed in a nematic liquid crystal K15 (4-cyano-4′-pentyl biphenyl) having the transition temperatures K-N: 23.8°C, N-I: 35.3°C (K – crystalline, N – nematic and I – Isotrop) provided by Merck [11], 5% b.w. In Table 1 is presented the composition of the studied samples.

The particles sizes have been analyzed by dynamic light scattering with the equipment Zetasizer Nano ZS (from Malvern). One notices from Table 1 that the dopant P5 has smaller particle dimension than P3.

In the resulted hybrids two ordered media interact: the organically modified layered silicates and the nematic liquid crystal.

Table 1. Composition of the studied samples

No.	COD/sample description	Particle description
1	Liquid crystal K15	–
2	K15/P3 Composite sample: K15/nanostratified copolymer sodium silicate DVB-MA (hybrid of K15 with DVB-MA and Cloisite Na)	Nanostratified particles of copolymer DVB-MA and Cloisite Na, Mean diameter 1020 nm
3	K15/P5 Composite sample: K15/ nanostratified copolymer DVB-MA-MEMNPEO$_4$ and Cloisite Na (hybrid of K15 with DVB-MA-MEMNPEO$_4$ and Cloisite Na)	Nanostratified particles of cloisite-DVB-MA, functionalized and stabilized Mean diameter 266 nm

The pure liquid crystal K15 and the mixtures were filled in 18 μm thick glass cell, having the glass plates covered with a transparent conductive Indium Tin Oxide (ITO) layer. The cells have been further used for electrical and electro-optical measurements.

2.2. *Experimental Set-Up*

2.2.1. *Scanning Electron Microscopy Image Acquisition.* The morphology of the mixtures was examined by scanning electron microscopy (SEM) with a FEI QUANTA 200 instrument, using low vacuum working mode and 20 kV accelerating voltage. A drop of the sample was placed on the stage of a Peltier device. The temperature was lowered to -5°C, with a cooling rate of 5°C/min, starting from room temperature. The sample was visualized after the sublimation of the ice formed on the stage. The morphology change was observed in the images registered in the $(-5 \div +20)$°C temperature range.

2.2.2. *Current-Voltage Curves.* The $I(V)$ measurements were made by using a Keithley 2400 electrometer, a temperature-controlled hot stage Mettler-Toledo 3200 series and an adequated homemade software [13].

2.2.3. *Electro-Optical Measurements.* The experimental set-up used to measure the optical response when applying different voltages and heating–cooling cycles has been described elsewhere [14,15]. In short, it contains a computer that controls the temperature variation rate of a home made hot stage and the applied voltage, a photomultiplier and a microscope. The light is transmitted through the sample placed between crossed polarizers and detected by a photomultiplier whose response U_{ph} is proportional to the input light intensity.

The thermal cycles applied on the sample are illustrated in Figure 1. In the first heating step (0), from room temperature T_0 to a pre-established temperature (T), higher than the nematic–isotropicic transition temperature of the liquid crystal, initial depolarization of the sample takes place. During the steps 1, 2, and 3 the polarizing field $E = 0$; these steps are performed to erase the eventual memory of the sample, by eliminating the eventually existing charges, due to previously treatments applied on the sample (manufacturing or previously applied heating cooling cycles and electric field).

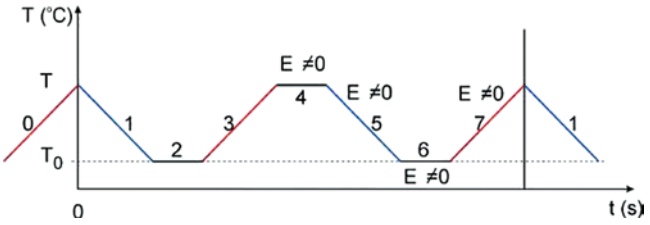

Figure 1. Heating-cooling cycles applied on the samples. (Figure appears in color online.)

During step 4, at temperature T, a polarizing field $E=U/g$ is applied, (where g is the thickness of the sample, U the applied voltage) and the LC dipoles orient. During steps 4,5,6,7 the same applied voltage is maintained and we measured the optical response by registering a photomultiplier signal. The heating-cooling rates were of 1°C/min, and the duration of steps 2, 4 and 6 where of 5 minutes. In this experiment, the polarization temperature is $T=50$°C and $T_0=25$°C.

2.2.4. *Measurements by Dielectric Spectroscopy.* In the aim to characterize the interaction of the liquid crystal and nanocomposites with the electric field, dielectric spectroscopy was applied as well. The equipment to measure the complex dielectric function was a high-resolution "Alpha" analyzer (Novocontrol, Germany) working in the frequency domain between 10^{-4} to 10^{7} Hz.

The complex dielectric permittivity was measured from 24 to 40°C at the following frequencies: 10 Hz, 100 Hz, 1 kHz, 10 kHz, 100 kHz and 1 MHz. Measurements were performed in one cycle of heating and cooling with 0.5°C/min continuous temperature ramp (with a precision better than 0.1°C). Temperature was controlled via a controller of the Quatro Cryosystem type (Novocontrol). Isothermal frequency scans were carried out as well on a series of temperatures with a stability better than 0.1°C. The complex dielectric function is defined by:

$$\varepsilon^*(f) = \varepsilon'(f) - i\varepsilon(f) \tag{1}$$

where $\varepsilon'(\omega)$ and $\varepsilon''(\omega)$ describe the real and imaginary part of the dielectric complex function [16]. Another quantity of interest is the complex conductivity which contains information on the d.c. conductivity and is related to the complex dielectric function by the relation:

$$\sigma^* = i\omega\varepsilon_0\varepsilon^* \tag{2}$$

The samples for dielectric measurements were sandwiched between two plane parallel circular electrodes at a distance of 50 μm (quartz fiber spacers) and measured either under an applied bias (+/−30 V) or without electric field.

3. Results and Discussions

3.1. *SEM Images*

In Figure 2a is presented the SEM image of the liquid crystal/nanostructured copolymer-clay K15/P3 and in Figure 2b, that of the K15/P5 system.

The SEM images although taken at the μm scale show a rather uniform distribution with well defined particles, despite the fact that the clay particles are

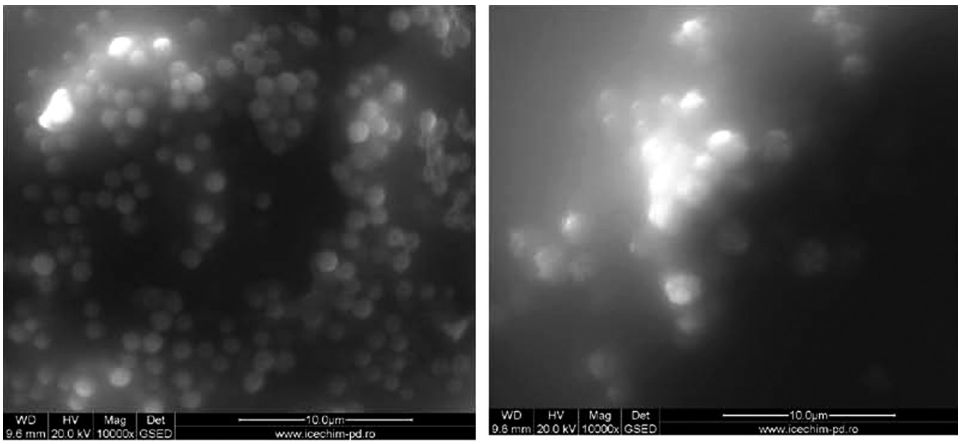

a) b)

Figure 2. (a) SEM images for K15/P3 and (b) for K15/P5 mixtures at temperature −5°C.

embedded in the organic material. The dimensions are consistent with the ones previously reported [10]. The mixture containing the P5 particles is more diffuse, because of a more intimate interaction with the liquid crystal and a greater total content of organic material of the P5 particles as compared to P3 particles.

3.2. *Electrical Measurements*

We have plotted the current-voltage (*I-V*) characteristics for a voltage range between −30 V and +30 V. The measurements have been performed in the nematic phase at 24 and 27°C and in the isotropic phase at 37°C. The results are presented in Fig. 3a) for the K15 liquid crystal, 3c) for the composite K15/P3 and 3e) for K15/P5. From the *I-V* plots we observe relatively small differences between the behavior in the nematic and isotropic phase.

We notice for all *I-V* representations a linear (Ohmic) variation, corresponding to lower applied d.c. electric fields and a nonlinear part, corresponding to higher values of electric field. Trying to linearize this part of the graph, we have plotted $\ln\left(I\sqrt{U}\right) = f(\sqrt{U})$ [17–21].

The distinct regions of the curves $\ln\left(I\sqrt{U}\right) = f(\sqrt{U})$ from Figure 3b and 3d might by interpreted in terms of the Schottky effect [22] (field-lowering of interfacial current at the injected electrode interface) in the first part of the *I(V)* curve, up to approx. $2 \cdot 10^5$V/m, and the Poole-Frenkel effect (field-assisted thermal detrapping of carriers), at greater electric fields.

For sample K15/P5 we have found a better linearization for the function $I = f(U^2)$, presented in Figure 3f. This might correspond to Mott's steady-state space-charge-limited conduction model [23].

3.3. *Electro-Optical Measurements*

We applied heating–cooling cycles on the samples as presented in Figure 1. In Figures 4a and b are presented the transmitted optical signal versus temperature for the liquid crystal K15 in step 5 (cooling) and step 7 (heating) respectively of

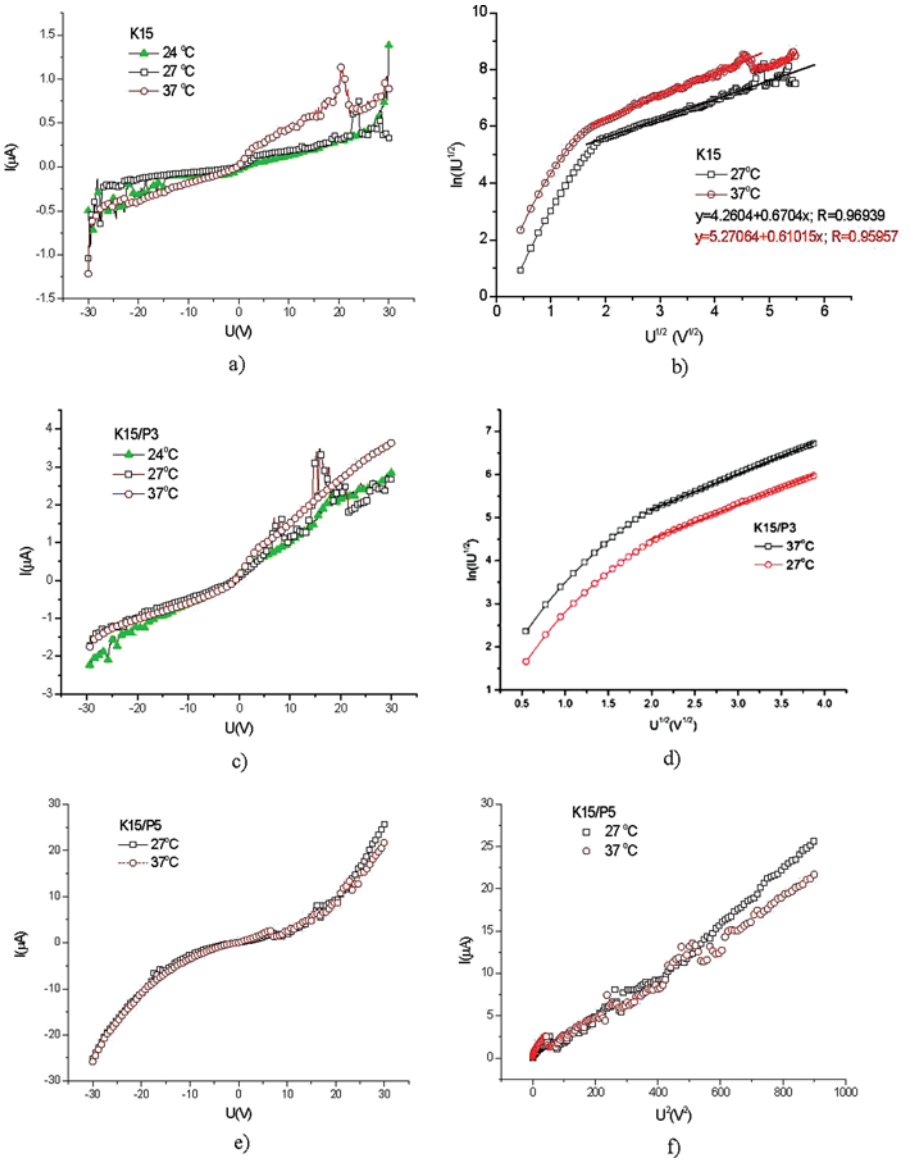

Figure 3. Current-voltage characteristics and corresponding $\ln(I\sqrt{U}) = f(\sqrt{U})$: (a) and (b) for K15 liquid crystal; (c) and (d) for K15/P3; (e) for K15; (f) graphic representation $I = f(U^2)$ for the K15/P5 sample. (Figure appears in color online.)

the heating–cooling cycles. In figures 4 c and d are presented the same for the composite sample K15/P3 while in Figs. 4 e and f) for the composite sample K15/P5.

Analyzing the curves presented in figures 4 one observes that:

a. the optical signal increases with the applied voltage at relatively small voltages, see Figures 4a and b (for U = 2 and 7 V) and Figures 4 e) and f) (for U = 2, 4 and 7 V). The same behavior was found for the system ZLI1221/P3 particle

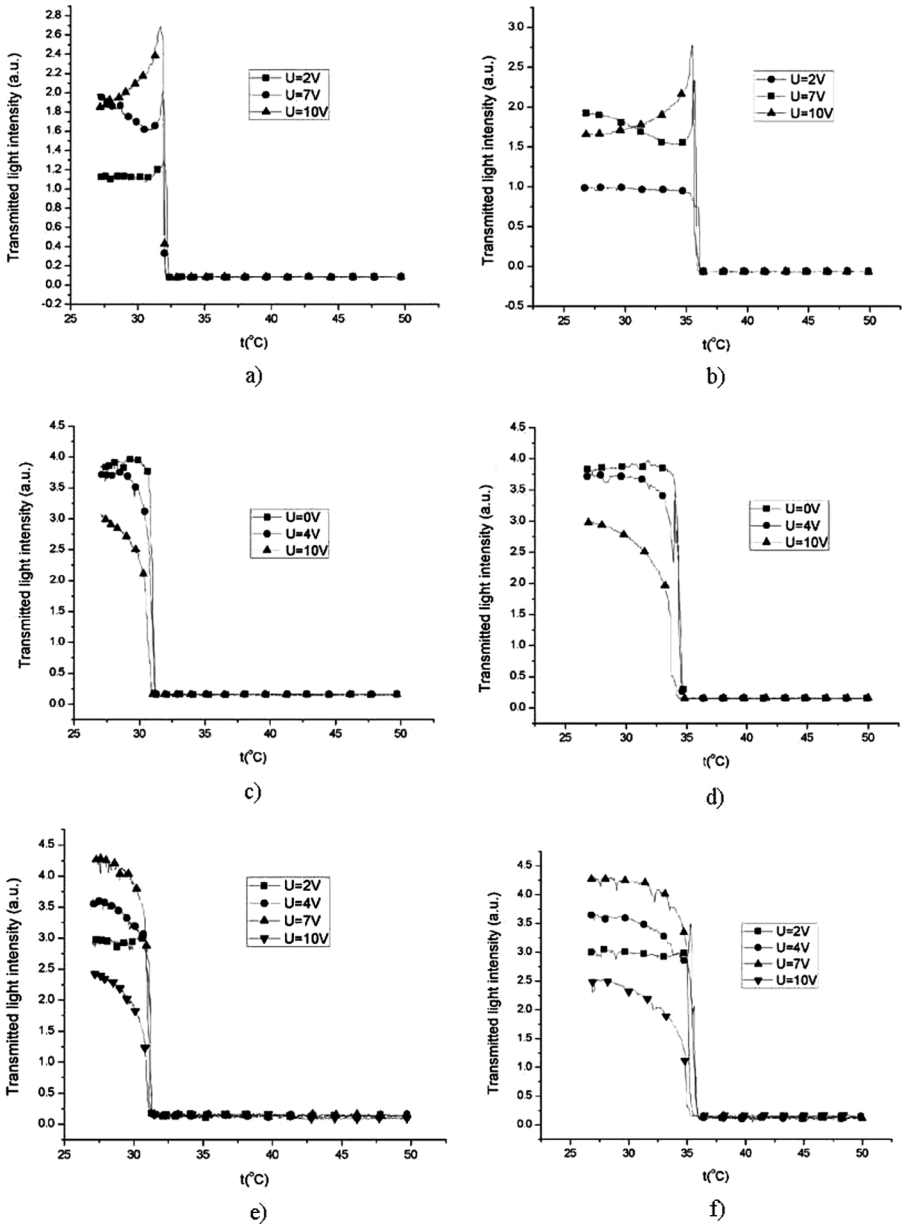

Figure 4. Transmitted light intensity versus temperature for different applied voltages: (a) liquid crystal K15, at cooling; (b) liquid crystal K15 at heating; (c) K15/P3 sample at cooling, (d) K15/P3 sample at heating; (e) K15/P5 sample at cooling; (f) K15/P5 sample at heating.

[12]. This can be explained as follows: by applying the electric field in step 5, an electrically induced order is superposed to the existing nematic order; according to [24,25] for K15 the dipole is along its molecular long axis. The more ordered system would have a higher optical transmission. Indeed, as observed for in Figures 4, up to a certain value, at the increase of the electric field, the

transmitted light intensity also increases. When further increasing the electric field, the optical transmission decreases. The phenomenon is more evident in Figures 4 b-e, at 10 V ($\sim 5 \cdot 10^5$ V/m) and as we have seen in section 3.2, at this value of the electric field, the shape of the current-voltage characteristics is nonlinear.

b. The transmittance of the composite samples is higher than that of the pure LC in the region of smaller temperatures, at variance of the behavior found for related systems such as carbon nanotubes or organomodified montmorillonit particles dispersed in 5CB [26,27], probably due to the different particle shape.

c. the nematic-isotropic transition observed by the detection of the optical signal takes place at temperatures greater than 35°C, when heating the sample, for all studied samples (see Figs. 4b,d,f). When cooling down the samples, the isotropic-nematic transition takes place at temperatures lower than 35°C.

For a better observation of this phenomenon, we studied the optical signal in a heating-cooling cycle, for 0 V applied voltage, for all samples. The results are presented in Figures 5.

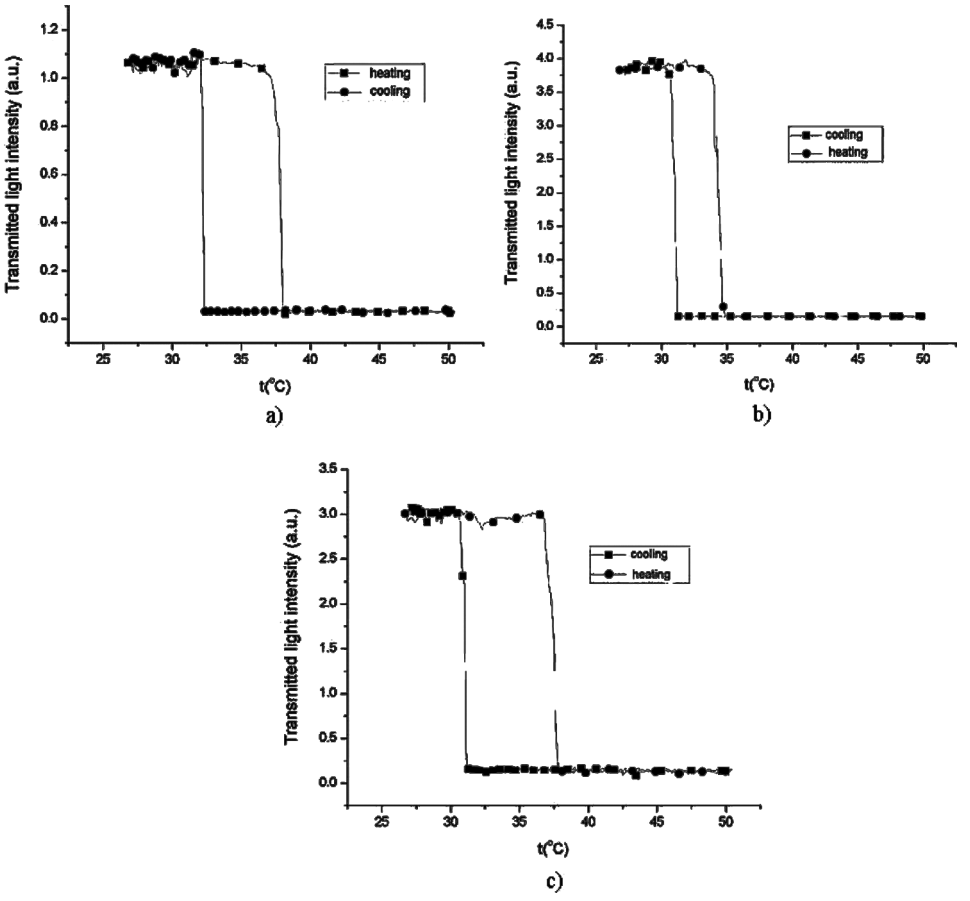

Figure 5. Hysteresis loop for the transmitted light obtained in heating-cooling cycles, without applied electric field for: (a) K15 liquid crystal; (b) K15/P3 sample; (c) K15/P5 sample.

These results confirm the previous observations, the N-I transition temperatures at heating are greater than the I-N transition temperatures when cooling. The scanning temperature rate being the same at heating and cooling (1°C/min), the system preserves the nematic order up to a higher temperature than the one reported in the literature, and when cooling down, it passes in the nematic phase to a relatively lower temperature.

3.4. *Measurements by Dielectric Spectroscopy*

The mixtures and the pure liquid crystal have been characterized by dielectric spectroscopy. The dielectric properties of bulk 5CB have been known for a long time. During the last decade such measurements were performed under special conditions (unaligned samples, enlarged frequency/temperature interval, high pressure) [28–31] or were related to the properties of complex composite systems [32–34]. In the liquid crystalline state due to its anisotropic structure several relaxation process are observed which are predicted also theoretically [35].

However, in order to characterize our samples and get new information useful for other electrical measurements, in this work we focus on the conductivity part.

In Figure 6 a 3D plot of the dielectric loss is given for the mixture K15/P3, as function of the frequency and temperature, as being representative for all the samples. As expected with increasing temperature the maximum of dielectric loss shifts to higher temperatures but at the temperature of the phase transition nematic-to-isotropic a jump is obvious in Figure 6.

A quick comparison of the investigated samples as concerning the dielectric loss dependence on the temperature, during the heating and cooling cycle, allowed the observation of a decrease of the nematic-to-isotropic transition temperature from K15 to K15/P5 and to K15/P3. This is an expected behavior and is sustained by other measurements.

To analyze the data quantitatively and to separate the different relaxation processes the model function of Havriliak-Negami (HN) [16] is employed as shown in figure 8a for the same sample considered in Figure 6. As it is known the

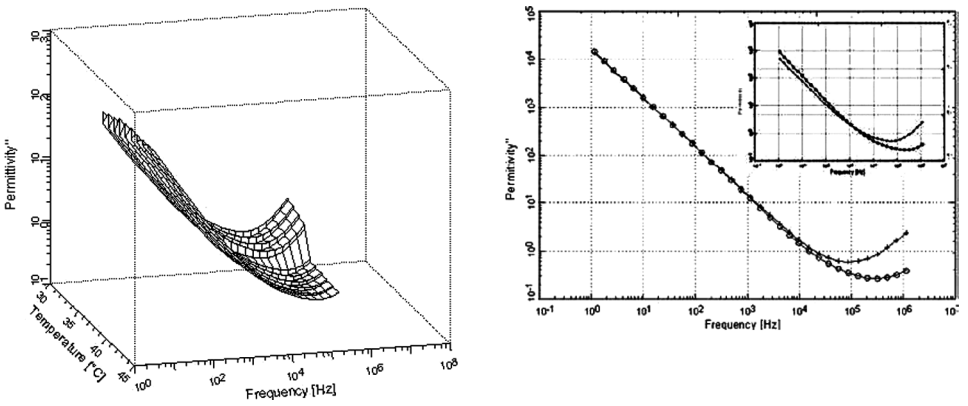

Figure 6. (a) 3D representation of the dielectric loss for the mixture K15/P3 at U=-30 V; (b) Variation of the dielectric loss with the frequency for U = 0 V and U = 30 V in the inset. The same sample as in part a.

HN-function reads

$$\varepsilon*(f) - \varepsilon_\infty = \frac{\Delta\varepsilon}{(1+(if/f_0)^\beta)^\gamma} \tag{3}$$

where f_0 is a characteristic frequency related to the frequency of maximal loss f_p (relaxation rate) of the relaxation process under consideration, ε_∞ describes the value of the real part ε' for $f \gg f_0$. β and γ are fractional parameters ($0<\beta\leq 1$ and $0<\beta\gamma\leq 1$) characterizing the shape of the relaxation time spectra. $\Delta\varepsilon$ denotes the dielectric strength, which is proportional to the mean squared effective dipole moment and to the number of the fluctuating dipoles per unit volume. Conduction effects were treated in the usual way by adding a conductivity contribution $\sigma_0/\varepsilon_0(2\pi f)^x$ to the dielectric loss. σ_0 is related to the d.c. conductivity of the sample and ε_0 is the dielectric permittivity of vacuum. The parameter x ($0<x\leq 1$) describes for $x<1$ non-Ohmic effects in the conductivity [16].

A typical decomposition is illustrated in Figure 7a where the arrows indicate the two model Havriliak-Negami functions and the calculated d.c. conductivity. The model functions represent two relaxation processes: one so-called hf (high frequency) process and the second lf (low-frequency) one. The continuous line passing through the experimental points represents the sum of the three above mentioned fitted components. These processes can be assigned to the relaxation of the LC molecules in the bulk phase and of the species upon the particle surface.

The variation of the calculated dc conductivity is represented in Figure 7b for the sample K15/P3, the same as in Figure 7a. The d.c. conductivity as resulted from the decomposition is lesser for an applied electric field than without it. In addition, the parameter x related to the conductivity contribution has values close to 1, indicating an Ohmic character of the conductivity. Moreover the slope of the plots in Figure 7b changes at the temperature of the phase transition.

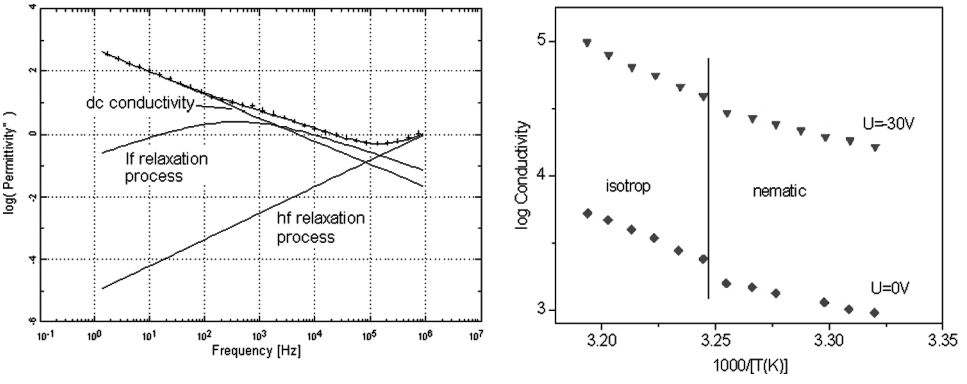

Figure 7. (a) Decomposition of dielectric spectrum (experimental points) into two model functions Havriliak-Negami (continuous curves) and a contribution of the d.c. conductivity (straight line). The spectrum belongs to K15/P3 sample at a temperature of 33.4°C, applied voltage being 30 V. (b) Conductivity variation with the inverse temperature for the sample K15/P3 at the indicated applied voltage. The vertical line shows the temperature of the phase transition in the bulk K15.

The found behavior is in agreement with the transport properties in nematic liquid crystal 4-cyano-4′-pentyl biphenyl [19]. Thus, it was discussed a charge injection from the electrode at the lower applied d.c. voltages, while the steady state current is due to the generation of mobile ions by the Poole-Frenkel effect in the bulk at the higher applied d.c. voltages.

The Ohmic behavior is foreseen by Naemura and Sawada [20] especially when high voltage was applied; the dissociation of ion pairs and the recombination of free ions could be the dominant mechanisms.

Conclusions

We have obtained new systems containing nematic liquid crystal/copolymer-clay composites. The nanostructured organic-inorganic particles were not treated with a surface surfactant after the polymerization. To ensure a good compatibility with the LC, a reactive surfactant was integrated in the particle structure during polymerization. The resulted liquid crystal-nanostructured composite hybrids form a complex structure, in which two ordered media interact: the organically modified layered silicates and the nematic liquid crystal.

The current-voltage curves show a linear (Ohmic) variation corresponding to lower values of the applied d.c. electric field, followed by a nonlinear region. After the linearization of these characteristics, we assumed that the Ohmic variation region might be attributed to the Schottky-like effect, while the nonlinear region to the Poole-Frenkel-like effect. For the sample containing liquid crystal doped with particles having integrated chemical groups compatible with the LC (“hairy” type), we found a variation that might be attributed to the Mott’s steady-state space-charge limited conduction model.

We applied consecutive heating-cooling cycles on the samples and different d.c. voltages and the transmitted light intensity were registered, showing an increase of the birefringence, at relatively moderate values of the d.c. electric field. When measuring the transmitted light in heating-cooling cycles with constant scanning temperature rate we found a thermal hysteresis behavior. The sample liquid crystal-functionalized copolymer-clay particles (K15/P5) show a better optical transmission when increasing the electric field, (at relatively moderate values), this fact and a good stability recommending the K15/P5 material for electro-optical applications.

In the aim to better characterize the interaction of the complex systems with the electric field, dielectric spectroscopy in the low frequency domain was also used. The sample temperature was varied between 24 and 40°C in a heating and cooling cycle. The measurements have shown that the temperature dependence of the dielectric loss is related to the nature of the sample and to the applied voltage. The results of the measurements performed with a low temperature variation rate, present hysteresis loops, similarly to the behavior of the transmitted light in the electro-optical experiments.

Acknowledgment

The authors acknowledge the financial support from CNCSIS – UEFISCSU, project PNII – IDEI ID_123/2008. Paul Ganea and Ligia Frunza thank the financial support by Core Program (Project PN09-45). We thank also the Merck Company for providing the liquid crystal.

References

[1] Kawasumi, M., Hasegawa, N., Usuki, A., & Okada, A. (1999). *Applied Clay Science*, *15*(1–2), 93–108.
[2] Chang, Y.-M., Tsai, T.-Y., Huang, Y.-P., Chen, W.-S., & Lee, W. (2007). *Japanese Journal of Applied Physics*, *46*(11), 7368–7370.
[3] Bezrodna, T., Chashechnikova, I., Nesprava, V., Puchkovska, G., Shaydyuk, Ye, Boyko, Yu., Baran, J., & Drozd, M. (2010). *Liq. Cryst.*, *37*(3), 263–270.
[4] Duijneveldt, J. S., Klein, S., Leach, E., Pizzey, C., & Richardson, R. M. (2005). *J. Phys.: Condens. Matter*, *17*, 2255–2267.
[5] Bezrodna, T., Chashechnikova, I., Dolgov, L., Puchkovska, G., Shaydyk, Ye., Lebovka, N., Moraru, V., Baran, J., & Ratajczak, H. (2005). *Liq. Cryst.*, *32*(8), 1005–1012.
[6] Jeong, E. H., Sun, K. R., Kang, M. C., Jeong, H. M., & Kim, B. K. (2010). *eXPRESS Polymer Letters*, *4*(1), 39–46.
[7] Tsai, T.-Y., Lee, C.-Y., Lee, C.-J., Chang, W. C., Lee, W., & Chen, P.-C. (2010). *J. Phys. Chem. Solids*, *71*, 595–599.
[8] Da Cruz, C., Sandre, O., & Cabuil, V. (2005). *J. Phys. Chem. B*, *109*(30), 14292–14299.
[9] Chashechnikova, I., Dolgov, L., Gavrilko, T., Puchkovska, G., Shaydyuk, Ye., Lebovka, N., Moraru, V., Baran, J., & Ratajczak, H. (2005). *J. Molec. Struct.*, *744–747*(3), 563–571.
[10] Somoghi, R., Donescu, D., Ghiurea, M., Radovici, C., Serban, S., Petcu, C., & Nistor, C. L. (2008). *J. Optoelectron. Adv. Mater.*, *10*(6), 1457–1462.
[11] Merck, Product Information, 10.02.1989.
[12] Rosu, C., Manaila Maximean, D., Donescu, D., Frunza, S., & Sterian, A. R. (2010). *Mod. Phys. Letts. B*, *24*(1), 65–73.
[13] Manaila Maximean, D., Bena, R., & Albu, A.-M. (1997). *Mod. Phys. Letts. B*, *11*(9–10), 431–440.
[14] Rosu, C., Manaila-Maximean, D., & Paraskos, A. J. (2002). *Modern Phys. Lett. B*, *16*(13), 473–483.
[15] Rosu, C., Manaila-Maximean, D., Godinho, M. H., & Almeida, P. L. (2002). *Mol. Cryst. Liq. Cryst.*, *391*, 1–11.
[16] Kremer, F., & Schönhals, A. (Eds.). (2003). *Broadband Dielectric Spectroscopy*, Springer-Verlag: Berlin-Heidelberg, 1–32.
[17] Murgatroyd, P. N. (1971). *J. Phys. D: Appl. Phys.*, *3*(2), 151.
[18] Mada, H., & Yamada, H. (1994). *Jap. J. Appl. Phys.*, *33*, 5886.
[19] Murakami, S., & Naito, H. (1997). *Jap. J. Appl. Phys.*, *1*(36), 773.
[20] Naemura, S., & Sawada, A. (2000). *Mol. Cryst. Liq. Cryst*, *346*(7), 155–168.
[21] Ongaro, R., & Pillonet, A. (1989). *Revue, Phys. Appl.*, *24*, 1085–1095.
[22] Abdel-Marlik, T. G., Abdel-Latif, R. M., Sawaby, A., & Ahmed, C. M. (2008). *J. Appl. Sci. Res.*, *4*(3), 331–336.
[23] Korneychuk, P. P., Gabovich, A. M., Voitenko, A. I., & Reznikov, Yu. A. (2009). *Ukr. J. Phys.*, *54*(1–2), 75–80.
[24] Picken, S. J., de Jeu, W. H., Picken, S. J., van Gunsteren, W. F., van Duijnen, P. Th., & de Jeu, W. H. (2006). *Liq. Cryst.*, *33*(11–12), 1359–1371.
[25] Nazario, Z., Sinha, G., & Aliev, F. (2001). *Mol. Cryst. Liq. Cryst.*, *367*, 333–340.
[26] Minenko, S. S., Kocherzhin, A. I., Lisetski, L. N., & Lebovka, N. I. (2009). *Funct. Mater.*, *16*, 319–323.
[27] Lisetski, L. N., Minenko, S. S., Fedoryako, A. P., & Lebovka, N. I. (2009). *Physica E*, *41*, 431–435.
[28] Urban, S., Kreul, H.-G., & Wurflinger, A. (1992). *Liq. Cryst.*, *12*, 921–930.
[29] Urban, S., Gestblom, B., & Dabrowski, R. (1999). *Phys. Chem. Chem. Phys.*, *1*, 4843–4846.

[30] Drozd-Rzoska, A., & Rzoska, S. J. (2002). *Phys. Rev. E*, *65*, 041701, 765–768.
[31] Belyaev, B. A., Drokin, N. A., & Shabanov, V. F. (2005). *Phys. Solid State*, 47.
[32] Różański, S. A., & Sinha, G. P. (2006). *J. Thoen, Liq. Cryst.*, *33*, 833–840.
[33] Rózański, S. A., Stannarius, R., Gorbatschow, W., & Kremer, F. (1996). *Liq. Cryst.*, *20*, 59–66.
[34] Leys, J., Glorieux, Ch., & Thoen, J. (2008). *Phys. Rev. E*, *77*, 061707.
[35] Jadzyn, J., Legrand, C., Czechowski, G., Bauman, D. (1998). *Liq. Cryst.*, *24*, 689–694.